

Fluid Evolution and Ore-forming Processes of the Jiama Cu Deposit, Tibet: Evidence from Fluid Inclusions

YAO Xiaofeng^{1,2,*}, LIU Jiajun¹, TANG Juxing³, ZHENG Wenbao³ and ZHANG Zhi⁴

¹ China University of Geosciences, Beijing 100083, China

² Development and Research Center, China Geological Survey (CGS), Beijing 100037, China

³ Key Laboratory of Metallogeny and Mineral Resources Assessment MLR, Institute of Mineral Resources, Chinese Academy of Geological Sciences (CAGS), Beijing 100037, China

⁴ Chengdu Institute of Geology and Mineral Resources, China Geological Survey, Chengdu 610082, Sichuan, China

Abstract: The Jiama deposit is a large copper deposit in Tibet. Mineralization occurs in three different host rocks: skarn, hornfels and porphyry. A detailed fluid inclusion study was conducted for veins in the different host rocks to investigate the relationship between fluid evolution and ore-forming processes. Based on examination of cores from 36 drill holes, three types of veins (A, B and D) were identified in the porphyries, four types (I, II, III and IV) in the skarn, and three (a, b and c) in the hornfels. The crosscutting relationships of the veins and that of the host rocks suggest two hydrothermal stages, one early and one late stage. Fluid inclusions indicate that the Jiama hydrothermal fluid system underwent at least two episodes of fluid boiling. The first boiling event occurred during the early hydrothermal stage, as recorded by fluid inclusions hosted in type A veins in the porphyries, type a veins in the hornfels, and wollastonite in the skarns. This fluid boiling event was associated with relatively weak mineralization. The second boiling event occurred in the late hydrothermal stage, as determined from fluid inclusions hosted in type B and D veins in the porphyries, type I to IV veins in the skarns, and type b and c veins in the hornfels. This late boiling event, together with mixing with meteoric water, was responsible for more than 90% of the metal accumulation in the deposit. The first boiling only occurred in the central part of the deposit and the second boiling event took place across an entire interlayered structural zone between hornfels and marble. A spatial zoning of ore-elements is evident, and appears to be related to different migration pathways and precipitation temperatures of Cu, Mo, Pb, Zn, Au and Ag.

Key words: fluid inclusion, fluid evolution, ore-forming processes, Jiama deposit, Tibet

1 Introduction

Numerous large and ultra-large mineral deposits have been discovered recently in the Gangdese Metallogenic Belt, Tibet. These include, for example, the Xiongkun, Qulong and Jiama deposits. The Jiama deposit is a large-scale Cu resource, and includes other metals such as Mo, Pb, Zn, Au and Ag (Tang Jvxing et al., 2010). Its origin has been proposed as a post-magmatic hydrothermal deposit related to calc-alkaline and high-K calc-alkaline magmatism (Ying Lijuan et al., 2009; Tang Jvxing et al., 2010; Qin Zhipeng et al., 2011). The Jiama deposit contains three main types of mineralization, including

porphyry, skarn and hornfels, and is characterized by elemental zonation from the center outward: Mo→Mo (Cu)→Cu (Mo)→Cu (Pb + Zn + Mo)→Cu (Pb + Zn)→Pb + Zn (Au) (Tang Jvxing et al., 2010; Zheng Wenbao et al., 2010; Yao Xiaofeng et al., 2014a).

A previous study was conducted on the Jiama deposit using a synchrotron radiation X-ray fluorescence microprobe to investigate individual melt inclusions from quartz phenocrysts in the porphyries (Zhou Yun et al., 2011a). The results revealed that Cu, Pb, Zn and other metallic elements were enriched in the vapor phase of inclusions (Zhou Yun et al., 2011a). Another study of fluid inclusions in both quartz phenocrysts and quartz veins within the granite porphyries, garnet, wollastonite and quartz veins in the skarns reconstructed the fluid

* Corresponding author. E-mail: 289332792@qq.com

evolution process that led to the formation of the skarn-type orebodies (Zhou Yun et al., 2011b). These studies provided the basis for resolving whether the deposit was to be classified as a submarine exhalative deposit or a magmatic-hydrothermal deposit (Zhou Yun et al., 2011a, 2011b).

However, two issues regarding the ore-forming processes of the Jiama deposit remain unresolved: the history of fluid evolution processes for the entire porphyry system, and the relationship between fluid evolution and ore-forming processes. Recent exploration efforts have revealed a number of different orebody types and an increased diversity of veins. These provide an ideal opportunity for more comprehensive study of the fluid evolution of the deposit. Based on detailed drill core logs, numerous veins within the porphyries, hornfels and skarns are identified and assigned to different mineralization

stages. Fluid evolution is examined by studying fluid inclusions from different mineralization stages, and the spatial distribution of fluids is analyzed using gangue minerals of the same stage from different locations within the deposit. This work aims to further develop understanding of the entire fluid evolution of mineralization and its relationship with ore-forming processes in the Jiama deposit.

2 Geological Setting

2.1 Regional geology

The Jiama deposit occurs within the south-central segment of the Gangdese Metallogenic Belt, located in the northern area of the Yarlung Zangbo Suture (YZS) (Fig. 1). Previous studies have shown that the major metallogenic series in the southern Gangdese Metallogenic

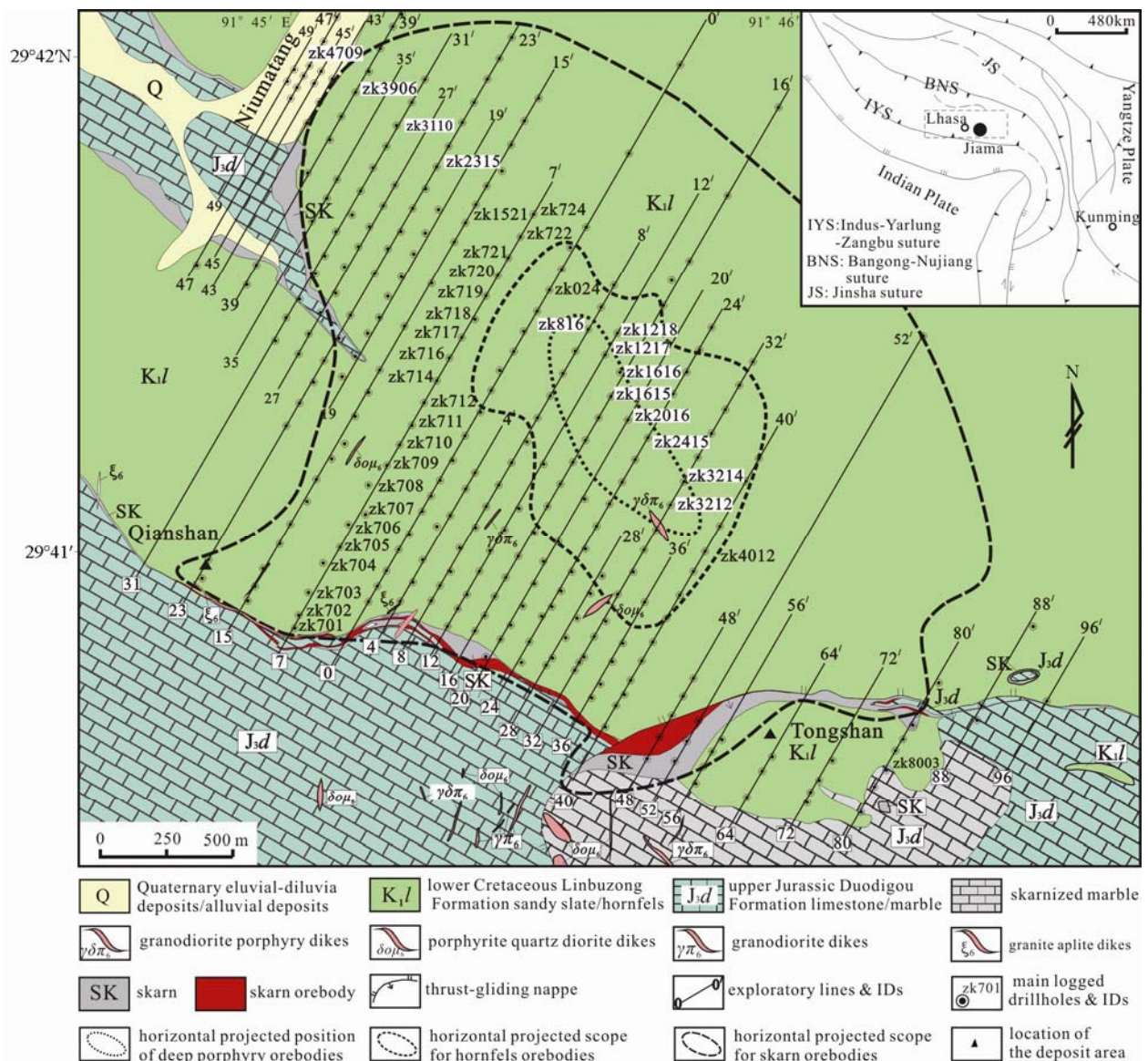


Fig. 1. Sketch geological map of the Jiama copper deposit (after Zheng Wenbao et al., 2011 and Ying et al., 2014).

Belt include four types that are related to the evolution of the Neo-Tethyan Ocean (Tang Juxing et al., 2012; Mao et al., 2014; Zheng et al., 2015). The first type is the Jurassic porphyry Cu-Au metallogenic series related to island arc magmatism, as represented by the Xiongkun deposit. This deposit is 175–160 Ma in age (Lang et al., 2014; Tang et al., 2015). The second type is the Cretaceous skarn Fe(-Cu) metallogenic series that occurs in a back-arc extensional setting (Zheng et al., 2015), as represented by the Nixiong skarn Fe deposit. This deposit has a mineralization age of 112 Ma (Yu Yushuai et al., 2012). The third type consists of the Paleocene-Eocene granitoid-related polymetallic metallogenic series that developed in a collisional setting. This type, represented by the Yaguila, Chagele, Jialong, Sharang, Bangbu, Leqingla and Xinga'guo deposits, mineralized in the 71–45 Ma age range (Gao Yiming et al., 2011; Wang Baodi et al., 2012; Huang Wenting et al., 2013; Wang et al., 2015; Zhao et al., 2015a; Pei Yingru et al., 2016). The fourth type is the Oligocene-Miocene porphyry-skarn Cu-W-Mo-Pb-Zn-Au-Ag metallogenic series that developed in a post-collisional setting (Chung et al., 2003; Hou et al., 2004; Gao et al., 2007; Qu et al., 2007; Hou et al., 2011;). This type is represented by the Nuri, Mingze and Chengba deposits that formed in the 40–20 Ma age range (Tang Juxing et al., 2012; Sun Xiang et al., 2013), and the Qulong, Zhibula, Chongjiang, Tinggong, Bangpu and Zhunuo deposits that mineralized in the 13.5–16.9 Ma age range (Meng Xiangjin et al., 2003; Rui Zongyao et al., 2003; Li Guangming and Rui Zongyao, 2004; Zhao et al., 2015b; Zhao et al., 2015; Xu et al., 2016; Huang Yong et al., 2017).

Molybdenite Re-Os isotopic ages and zircon U-Pb ages of mineralization-related intrusive rocks in the Jiama deposit indicate that mineralization took place between 16 and 14 Ma (Ying Lijuan et al., 2009; Qin Zhipeng et al., 2011; Ying Lijuan et al., 2011; Ying et al., 2014; Zeng Zhongcheng et al., 2016) in a post-collision setting. The Jiama deposit is located in the Jiama-Kajunguo thrust-gliding nappe fold-fault system (Zhong Kanghui et al., 2012), where the D₂ structural deformation, coeval with mineralization, is believed to have significantly affected ore enrichment (Duan et al., 2014). The mineralization-related magmatic system is interpreted to have resulted from mixing of re-melted granitic magma from the upper crust with dioritic magma from the lower crust (Tang Juxing et al., 2010; Qin Zhipeng et al., 2011).

2.2 Ore deposit geology

The strata that crop out in the Jiama deposit area mainly include sandy slate and hornfels of the Lower Cretaceous Linbuzong Formation (K₁l) and limestone and marble of

the Upper Jurassic Duodigou Formation (J₃d). Only a small amount of Quaternary sediments occur in Niumatang (Fig. 1). Intrusive rocks typically occur as dikes, and consist of granite, monzonitic granite, granodiorite, quartz diorite and diorite porphyries, as well as spessartite and proterobase (porphyrite). Intrusion of the granite porphyry is closely related to mineralization, and typically occurs at depths between exploratory lines 8 and 36 (Fig. 1). Mineralization mainly occurs as polymetallic Cu in the skarn, Cu-Mo in the hornfels and Mo (Cu) in the porphyry (Yao Xiaofeng et al., 2014a, 2014b).

2.2.1 Orebodies and veins in skarns

Skarn orebodies are primarily hosted in the interlayered structural zones between sandy slate/hornfels (roof) and limestone/marble (floor). They mainly occur in stratoid and stratiform forms that extend for 4200 m along strike (NE 30°) and almost 2500 m along dip (Ying et al., 2014). The orebodies dip steeply (50–70°) at shallow depths, but more moderately (10–20°) at greater depths (Fig. 2). Ore minerals occur as disseminations, massive bodies and veins. The main economic ore minerals are molybdenite, chalcopyrite, bornite, tetrahedrite, chalcocite, galena and sphalerite. Gangue minerals include garnet, wollastonite, diopside, tremolite, chlorite, epidote, quartz and calcite.

Four types of veins are found in the skarns: quartz + sulfide (type I), wollastonite + quartz + sulfide (type II), quartz + garnet ± wollastonite ± epidote ± sulfide (type III) and quartz ± garnet ± sulfide (type IV) (Fig. 3e–h). Type I veins have clear wall rock contacts, and mainly dip at less than 40°. Widespread irregular occurrences of type I veins are evident in drill cores from the deposit. Type II, III and IV veins are primarily found close to the porphyry center and have regular morphology, and some veins dip steeply (>70°). Garnet, wollastonite, chlorite and epidote are observed in the outer edges of type II, III and IV veins. Type I veins in the skarns are transected by type II, III or IV veins (Fig. 3e).

2.2.2 Orebodies and veins in hornfels

Hornfels within the deposit area is a product of thermal metamorphism induced by intrusions, and covers a maximum area of about 40 km² (Wang Denghong et al., 2011). Hornfels orebodies, related to the porphyry system, are mainly found above the porphyry intrusions (Fig. 2) close to the center of the deposit. The main orebodies occur as massive, irregular and vertically-orientated cylindrical forms in the roof of skarns. The main orebody is 1.2 km long and about 0.8 km wide (Fig. 1) with a maximum thickness of about 900 m (Tang Juxing et al., 2010; Leng Qiufeng et al., 2014). Ores typically occur in veins or stockworks, similar to the main ore structures of

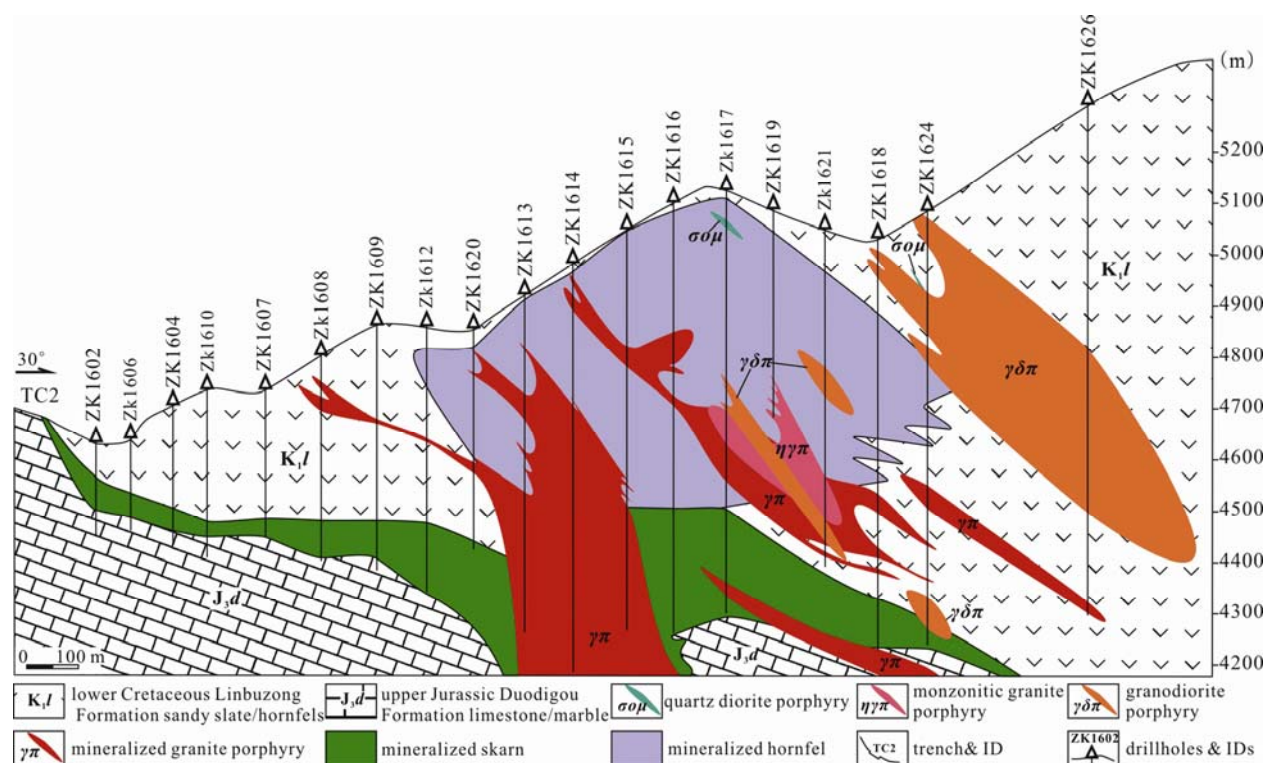


Fig. 2. No. 16 geological section of the Jiama deposit (modified from Tang Jvxing et al., 2013)

the porphyry orebody. Economic ore minerals include chalcopyrite and molybdenite, and gangue minerals include quartz, feldspar, biotite and chlorite.

Three types of veins have been identified in hornfels orebodies from core logs: quartz + biotite halo/chlorite halo/silicified halo ± pyrite ± pyrrhotite ± chalcopyrite (type a); quartz + biotite halo/chlorite halo/silicified halo + pyrite ± chalcopyrite ± molybdenite (type b) and quartz ± pyrite ± chalcopyrite ± molybdenite (type c) (Fig. 3c–d). Type a veins, which are widespread in the deposit area, are typically developed along bedding and are parallel to each other, with irregular morphology and diffuse wall rock contacts. Alteration halos prevail in the exterior of the veins. Type b veins transect bedding and have regular morphology and diffuse wall rock contacts. Alteration halos are commonly found along the vein walls. Type b veins are mainly found close to the intrusion center. Type c veins occur with regular morphology and distinct wall rock contacts with no alteration halos developed on the outer vein edges. Type c veins transect type a and b veins (Fig. 3c–d), and are most abundant near the intrusion center.

2.2.3 Orebodies and veins in porphyries

Porphyry orebodies are developed across the entire, deeply-buried granite porphyry between lines 8 and 32. The orebodies appear as long shuttle-shaped bodies in plane projection. The projection of the main orebody is 0.8

km long and 0.2 km wide (Fig. 1), and occurs in an irregular or forked form at depth. The proven thickness of the orebody from the drill logs is in the 14.1–361.1 m range. However, its extension at depth has not been controlled by exploration yet (Fig. 2). The ores occur primarily in veins or stockworks, and the main ore minerals include molybdenite and chalcopyrite, with gangue minerals of quartz, feldspar, biotite, sericite and chlorite.

Most porphyry Cu deposits have at least four groups of veins (Dilles and Einaudi, 1992; Gustafson, 1995; Cannell, 2005; Sillitoe, 2010), with the first group involving early sulfide-free quartz veins with actinolite/biotite (EB veins). These veins show no sign of alteration boundaries. The second group of veins involves sub-early quartz sulfide veining (type A veins) with irregular boundaries. Quartz occurs in these veins in granular form, and biotite or K-feldspar alteration boundaries are developed. The third group involves sub-late quartz sulfide veining (type B veins) with relatively regular boundaries, granular quartz, and alteration halos of biotite, chlorite or sericite. The fourth group are latest quartz sulfide veins that have straight boundaries (type D veins), with well-crystallized quartz veins and no alteration halos.

Based on these criteria, type EB, A, B and D veins are identified in the Jiama deposit. Early biotite veins with thin and irregular morphology are the type EB veins. The irregular veins with diffuse wall rock contacts are the type

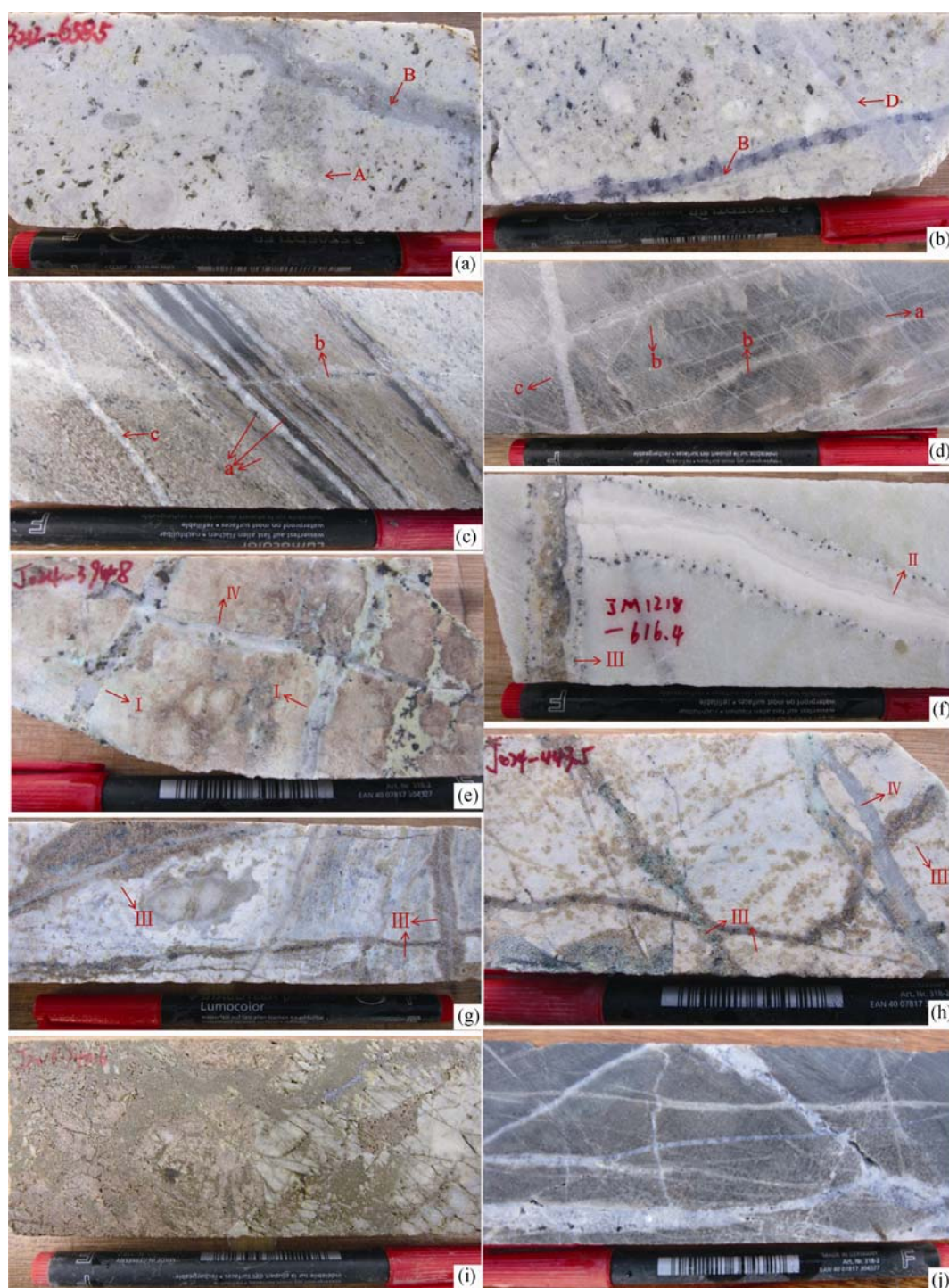


Fig. 3. Features and crosscutting relationships of various types of veins in porphyries, hornfels and skarns from the Jiama deposit

(a), Type A vein (quartz + sericite + chalcopyrite + pyrite) are cut by type B vein (quartz + biotite halo + chlorite halo) in granite porphyry, from drill core J3212 at 658.5 m; (b), Type B veins (quartz + molybdenite) in granite porphyry are cut by type D veins (barren quartz vein), from drill core J3212 at 650.2 m; (c), Along-bedding type a veins (quartz + biotite halo + chalcopyrite + pyrite, quartz + chalcopyrite + pyrite) in hornfels are cut by type b veins (quartz + chalcopyrite + pyrite), from drill core J024 at 223.6 m, while type b veins are cut by type c veins (quartz + molybdenite); (d), Type b veins (quartz + biotite halo + chalcopyrite + pyrite, quartz + chlorite halo) are cut by type c veins (barren quartz), from drill core J4012 at 251.3 m; (e), Type I veins are cut by type IV in skarn, from drill core J024 at 394.8 m; (f), Type II veins (quartz + wollastonite + bornite) in marble are cut by type III veins (quartz + almandite + wollastonite + bornite), from drill core J1218 at 616.4 m; (g), Two forms of type III veins (quartz + almandite + bornite) in garnet wollastonite skarn, from drill core J3212 at 631.8 m; (h), Type III veins (quartz + almandite + bornite) are cut by type IV veins (barren quartz vein) in skarn, from drill core J024 at 443.5 m; (i), Skarn is cryptoexplosively brecciated, from drill core J2016 at 740.6 m; (j), Stockwork structure in hornfels, from drill core J1217 at 475.3 m.

A veins that contain albite, K-feldspar and sericite halos at the outer vein edges. The halos are primarily in the form of quartz + K-feldspar and quartz + sericite (\pm chalcopyrite \pm pyrite) (Fig. 3a). The latter are the most common. The irregular morphology veins with relatively clear boundaries are the type B veins. These contain biotite and chlorite halos at the outer vein edges, primarily in the form of quartz + biotite (\pm chalcopyrite \pm pyrite), quartz + chlorite (\pm chalcopyrite \pm pyrite), quartz \pm anhydrite + chalcopyrite + molybdenite and quartz + molybdenite (Fig. 3a–b). The latter are the most common ore-hosting form in the porphyry orebodies. Type D veins are rare, occurring only as regular-shaped tabular veins that contain quartz + molybdenite and barren quartz veins (Fig. 3b).

2.2.4 Hydrothermal mineralization stages

Crosscutting relationships of type A, B and D veins in porphyries, type a, b and c veins in hornfels and type I, II, III and IV veins in skarns provide important information with which to sub-divide the stages of mineralization in the Jiama deposit. Skarn mineralization is commonly divided into three stages: prograde skarn stage, retrograde alteration stage and sulfidization stage. For the skarn in the Jiama deposit, garnet, diopside and wollastonite formed during the prograde stage, while epidote and chlorite formed during the retrograde alteration stage. Quartz, sulfides and different type of veins formed during the sulfidization stage. However, more orebodies and veins

are evident in the porphyries and hornfels of the Jiama deposit, and so these hydrothermal products need to be taken into consideration. Brecciated zones mainly occur in the skarn and granite porphyries, and consist of fragments of garnet skarn, wollastonite skarn and marble cemented by quartz. Above the brecciated zone, type II/III/IV veins in the skarn and type b/c veins in the hornfels are more abundant close to the brecciated zone. Conversely, type B/D veins are more developed under the brecciated zone in the granite porphyry, close to the brecciated zone. It can be inferred that these types of veins formed synchronously or later than brecciation, and prograde skarn and retrograde alteration minerals and type a veins formed before brecciation. As proposed by Sillitoe (2010), type A veins in porphyries are commonly considered to be products of plastic deformation prior to brecciation that occurs during magmatic-epithermal evolution. This study is mainly focused on the evolution of hydrothermal fluids after the magmatic-hydrothermal transition. The hydrothermal mineralization process can be divided into two stages: early hydrothermal (Stage 1) and late hydrothermal (Stage 2) (Fig. 4).

3 Samples and Methods

Two groups of samples were collected: the first group from the central part of the deposit and the second from type a and type I veins in different locations. The first group contains garnet, wollastonite and quartz from

Mineralization stage	pre-hydrothermal stage	early hydrothermal stage	late hydrothermal stage
porphyry	magmatic minerals	type A	type B type D
skarn	prograde skarn minerals	retrograde alteration minerals	type I type II type III type IV
hornfels		type a	type b type c
brecciation			

Fig. 4. Paragenetic sequence of the mineral assemblages and veins of the Jiama deposit, based on crosscutting and brecciation relationships.

different stages and from different host rocks (porphyries, skarns and hornfels). Samples from the type a veins in skarns were collected from the center of the deposit (lines 7–40) outwards, from drill holes J4012, J3214, J2415, J1217, J024, J721, J1521, J2315, J3110 and J3906 (Fig. 1). Samples from the type I veins in skarns were collected from drill holes ZK721, ZK719 and ZK714 in the central part of the deposit, and from ZK708, ZK705 and ZK703 in the outer part (Fig. 1).

Petrographic and microthermometric studies on fluid inclusions were conducted using a THMSG600 system (Linkam Scientific Instruments, Surrey, United Kingdom). The cooling-heating stage was calibrated using standard synthetic fluid inclusions provided by FLUID Inc, with an accuracy of $\pm 2^\circ\text{C}$ for the 0–600°C interval and $\pm 0.5^\circ\text{C}$ for the -196 – 0°C interval. The fluid inclusion microthermometry workflow was as follows: photography → freezing → heating. The fluid inclusions were generally cooled to between -70°C and -120°C at a rate of $20^\circ\text{C}/\text{min}$ until frozen. The re-heating rate was $15^\circ\text{C}/\text{min}$, and was adjusted to 2 – $5^\circ\text{C}/\text{min}$ when the temperature reached -30°C . When the temperature was close to the point at which the last ice crystal disappeared, the warming rate was reduced to 0.1 – $0.5^\circ\text{C}/\text{min}$, and the freezing temperature was duly recorded. After the freezing process was completed, the temperature was continuously increased at a rate of $25^\circ\text{C}/\text{min}$. When the temperature reached 100°C , the heating rate was adjusted to $10^\circ\text{C}/\text{min}$. When the temperature was close to the point of homogenization (or the solid phases disappeared), the heating rate was reduced to 2 – $3^\circ\text{C}/\text{min}$. The inclusions were heated continuously until the solid phases or the vapor disappeared, and the respective temperatures were

recorded. The salinities of the fluid inclusions were calculated using the formula of Hall et al. (1988), but some inclusions did not yield freezing temperatures because of their small size. All salinities are reported as wt% NaCl eq. unless otherwise stated.

4 Results

4.1 Fluid inclusion petrography

Based on the phase assemblages at room temperature, the fluid inclusions from the Jiama deposit can be divided into two types: type i and type ii. Type i inclusions are composed of liquid and/or vapor, without solid phases, whereas type ii inclusions contain solid phases in addition to fluid phases.

Type i inclusions are divided into two sub-types, type i-1 and type i-2. The type i-1 inclusions consist of liquid and vapor with vapor contents of 5–60% (Fig. 5a, c), and homogenize into the liquid phase. These inclusions are typically 5–25 μm in size and are circular, elliptical, rice-shaped or irregular in shape. They are well-developed in different stages of veins, and account for 40–60% of the total fluid inclusion population. Type i-2 fluid inclusions have vapor percentage of 60–100% (Fig. 5a, d), and homogenize into the vapor phase. They are 10–50 μm in size and are elliptical or irregular in shape. They account for 10–20% of the total fluid inclusion population.

Type ii inclusions have at least three phases (liquid, vapor and solid) at room temperature. They are 5–40 μm in size (mostly 15–30 μm) and are elliptical or irregular in shape. The most common solid phase is halite, although sylvite and sulfides are also observed in some inclusions. Halite crystals are mostly cubic in shape, light green in

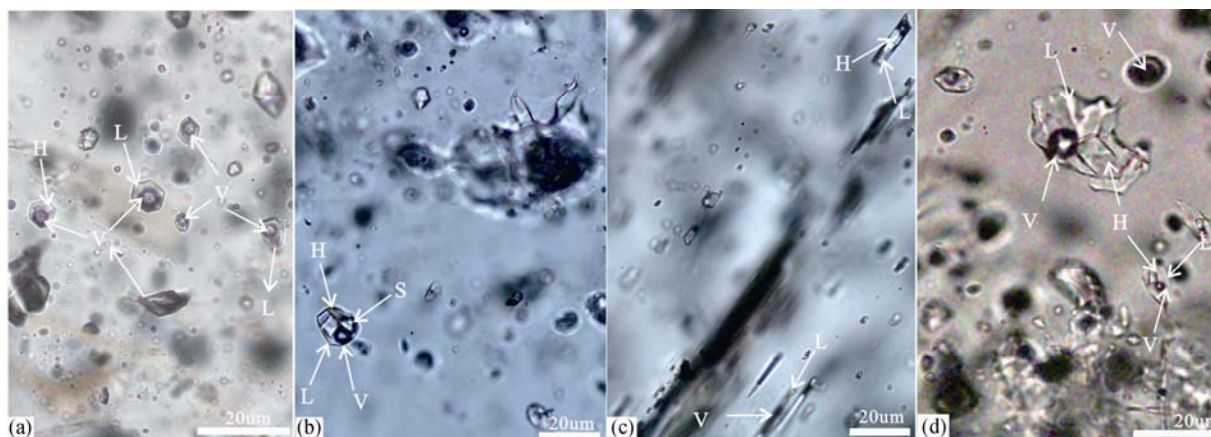


Fig. 5. Petrographic features of different types of fluid inclusions from gangue minerals in porphyries, skarns and hornfels, Jiama deposit.

(a), Two-phase and three-phase inclusions with different vapor/liquid ratios in type B vein, J3214-616.4, granite porphyry; (b), Multiphase inclusions with halite and sylvite crystals in type a quartz veins, J024-127, hornfels; (c), Two-phase and three-phase inclusions within wollastonite, J4012-743.5, skarn; (d), Two-phase and three-phase inclusion groups in type I veins, J708-196.3, skarn; V, Vapor; L, Liquid; H, Halite solid phase; S, Sylvite solid phase.

color, and normally $<10\ \mu\text{m}$ in size. Sylvite crystals are typically circular or rectangular in shape, while the sulfides are generally very small, and occur in irregular or triangular shapes. Some of the type ii inclusions have only one solid phase (Fig. 5c, d), whereas some may have multiple solid phases (Fig. 5b). The type ii inclusions can also be divided into two subtypes: type ii-1 inclusions, in which the solid phases dissolve before the vapor phase disappears during heating, and type ii-2 inclusions, in which the vapor phase disappears before the solid phases dissolve.

The fluid inclusion assemblage (FIA) concept of Goldstein and Reynolds (1994) was used to verify the consistency of the microthermometric data. Fluid inclusion assemblages in vein quartz are distributed within crystal growth zones (Fig. 6c, e, g) and occur as trails along healed fractures which do not cut across quartz crystal boundaries (Fig. 6i). Some are clustered, isolated or scattered inclusions (Fig. 6a) that are interpreted to be of pseudo-secondary or primary origins, and were mainly chosen for investigation in this study. Fluid inclusion assemblages in wollastonite occur along growth zones and are of primary origin (Fig. 6b). Most of the fluid inclusions studied in garnet are isolated or distributed in intracrystal healed fractures. These are interpreted to be of primary or pseudo-secondary origins. Only potential primary or pseudo-secondary inclusions were examined, with secondary fluid inclusions (those distributed along long, intercrystal fractures) being excluded. Further, microthermometric data with a difference of homogenization temperature (T_h) values $>15^\circ\text{C}$ within a small area were not adopted, even if they could be unambiguously defined as an FIA (Chi Guoxiang and Lu Huanzhang, 2008).

The coexistence of type i-1, i-2 and ii fluid inclusions within individual fluid inclusion assemblages, found in all veins types close to the center of the deposit (Fig. 6) is interpreted to indicate fluid boiling. This is commonly observed in quartz of type I veins throughout line 7 in the deposit, but for type a veins in hornfels, boiling is only evident in the center of the deposit. Additionally, fluid inclusions in type a veins decrease significantly in abundance and size toward the periphery, and very few inclusions $<2\ \mu\text{m}$ were found in type a veins in drill cores J3110 and J3906.

4.2 Homogenization temperature and salinity

Overall, the studied fluid inclusions have homogenization temperatures in the $201\text{--}459^\circ\text{C}$ range, and salinities in the $1.1\text{--}43.4\ \text{wt}\%$ NaCl eq. range (Table 1). In porphyries, fluid inclusions in gangue minerals from different stages have homogenization temperatures in the

$249\text{--}392^\circ\text{C}$ range, with salinities in the $3.1\text{--}36.5\ \text{wt}\%$ range. In hornfels, fluid inclusions in gangue minerals from different stages have homogenization temperatures in the $240\text{--}459^\circ\text{C}$ range, with salinities in the $2.1\text{--}43.3\ \text{wt}\%$ range. In skarns, fluid inclusions from garnet and wollastonite have homogenization temperatures in the $308\text{--}455^\circ\text{C}$ range, with salinities in the $4.3\text{--}43.4\ \text{wt}\%$ range. Fluid inclusions from quartz in different veins have homogenization temperatures primarily in the $224\text{--}404^\circ\text{C}$ range, with salinities in the $1.1\text{--}36.9\ \text{wt}\%$ range. These data are presented in Table 1 and Fig. 7.

Within gangue minerals of the early hydrothermal stage, type i fluid inclusions have T_h values in the $245\text{--}455^\circ\text{C}$ range, with salinities in the $2.6\text{--}22.5\ \text{wt}\%$ range. Type ii fluid inclusions have T_h values in the $240\text{--}410^\circ\text{C}$ range, with salinities in the $30.2\text{--}43.4\ \text{wt}\%$ range. Within gangue minerals of the late hydrothermal stage, type i fluid inclusions have T_h values in the $237\text{--}453^\circ\text{C}$ range, with salinities in the $2.1\text{--}20.5\ \text{wt}\%$ range. Type ii fluid inclusions have T_h values in the $237\text{--}459^\circ\text{C}$ range, with salinities in the $31.1\text{--}43.0\ \text{wt}\%$ range. These data are presented in Table 1 and Fig. 8. Generally, for fluid inclusions from early to late stages, the homogenization temperatures gradually decrease and the salinities change diversely because of boiling, cooling and dilution (Fig. 8).

Fluid inclusions from type a veins in the center of the deposit (lines 7–40) have homogenization temperatures in the $240\text{--}413^\circ\text{C}$ range and salinities in the $2.6\text{--}43.3\ \text{wt}\%$ range. On the periphery of the deposit, no reliable inclusion data were acquired from type a veins in J3110 and J3906 drill holes. Fluid inclusions in samples from J2315 and J1521 drill holes have homogenization temperatures in the $244\text{--}348^\circ\text{C}$ range and salinities in the $0.9\text{--}2.4\ \text{wt}\%$ range (Table 1, Fig. 9). Fluid inclusions from type I veins in the center of the deposit have homogenization temperatures in the $224\text{--}379^\circ\text{C}$ range and salinities in the $1.1\text{--}34.1\ \text{wt}\%$ range, while those from type I veins on the periphery are in the $210\text{--}386^\circ\text{C}$ range and $1.4\text{--}34.9\ \text{wt}\%$ range, respectively (Table 1, Fig. 10).

5 Discussions

5.1 Fluid evolution

The magmatic-hydrothermal transition stage can be considered the initial stage of fluid evolution. Generally, unidirectional solidification texture (UST), quartz eyes, cavities and other similar microstructures within intrusions are considered as geological records, while melt inclusions that coexist with fluid inclusions in early quartz veins or quartz phenocrysts can give more direct information about magmatic-hydrothermal transition (Harris et al., 2003, 2004). Zhou Yun et al. (2011a) found that homogenization

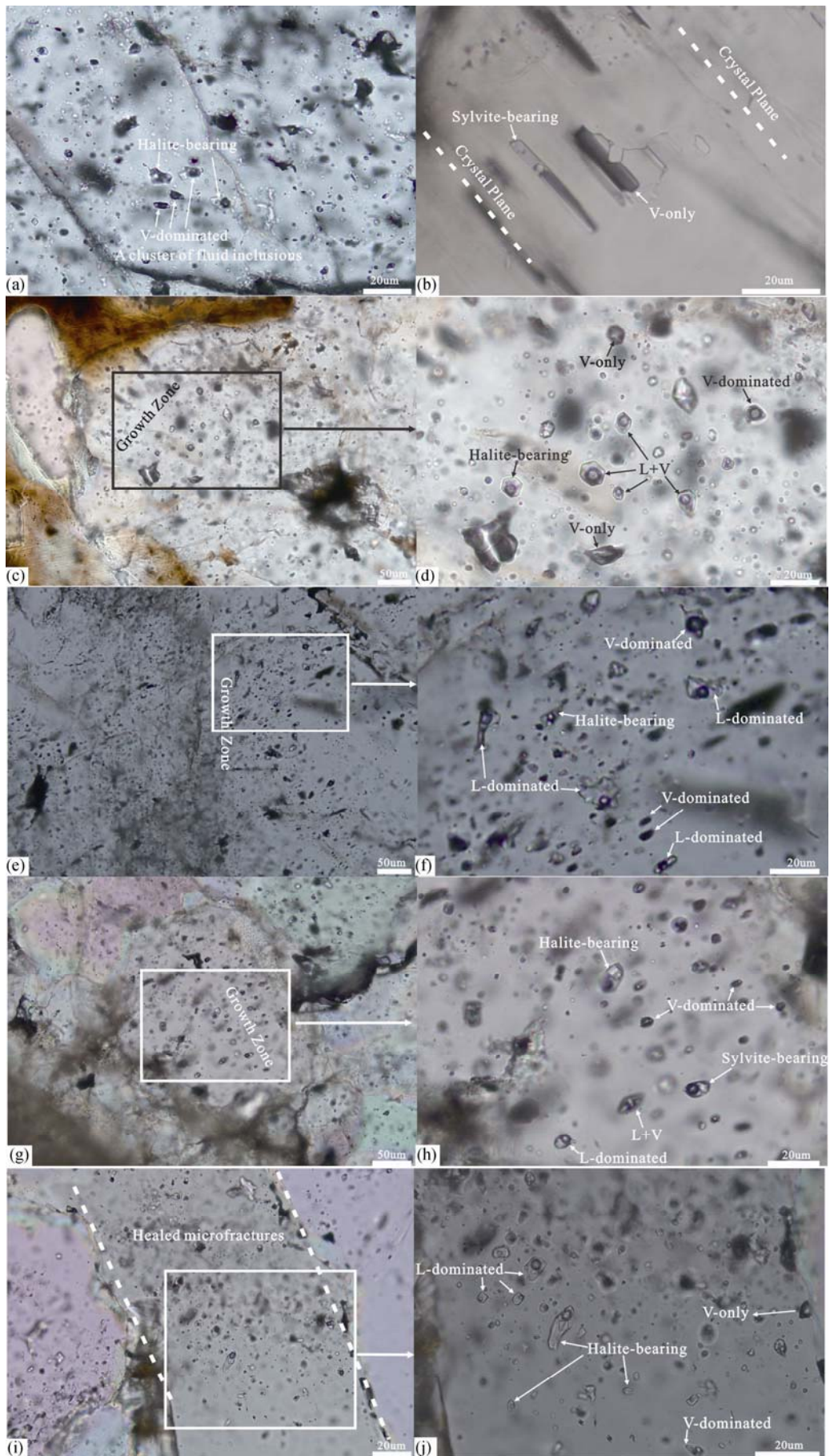


Fig. 6. Photomicrographs showing occurrences of coexistence of different types of inclusions within individual fluid inclusion assemblages in porphyries, skarns and hornfels.

(a), A cluster of fluid inclusions showing coexistence of vapor-dominated and halite-bearing fluid inclusions in type A quartz veins within granite porphyry, J3212-658.5; (b), Coexistence of vapor-only and sylvite-bearing fluid inclusions, parallel to crystal plane, in wollastonite of the skarn stage, J711-1144; (c), A group of fluid inclusions in a growth zone in type B quartz veins within granite porphyry, J3214-616.4; (d), Enlargement of the fluid inclusions in c; (e), A group of fluid inclusions in a growth zone in a type I quartz vein within skarn, J716-255.2; (f), Enlargement of fluid inclusions in e; (g), A group of fluid inclusions in a growth zone in a type a quartz vein within hornfels, J4012-463.2; (h), Enlargement of fluid inclusions in g; (i), A group of fluid inclusions within healed microfracture in a type c quartz vein within hornfels, ZK024-127; (j), Enlargement of fluid inclusions in i.

Table 1 Fluid inclusion microthermometric data for the Jiama deposit

Stage	Location	Mineral	Type	Vapor (%)	T_h (°C)	T_{ice} (°C)	T_v (°C)	T_s (°C)	Salinity (% NaCl eq.)			
Stage 1	Center	type A quartz vein	i-1	10–30	295–371	–9 to –10.1			12.9–14.1			
			i-2	60–80	310–392	–2.6			4.3			
			ii-1	10–30	265–309			218–277	32.8–36.5			
			garnet	i-1	5–20	363–455						
				i-2	50–70	389–417						
				ii-1	15–30	380–418			245–291	34.4–37.5		
		wollastonite	i-1	10–40	315–389							
			i-2	60–70	333–375	–2.9 to –3.9				4.8–6.3		
			ii-1	10–20	367–401				307–360	38.7–43.4		
			i-1	10–40	269–413	–2.7 to –20.1				4.5–22.5		
			type a quartz vein	i-2	60–90	245–387	–1.5 to –5.2				2.6–9.6	
				ii-1	10–40	240–410				164–359	30.2–43.3	
		Periphery	type a quartz vein	ii-2	20–40	262–410			205–356	32.1–43.1		
				i-1	5–15	243–341	–0.5 to –1.4				0.9–2.4	
		Stage 2	Center	type B quartz vein	i-1	5–40	249–363	–1.8 to –4.1				3.1–6.6
					i-2	70	277–365	–2.1 to –2.9				3.6–4.8
					ii-2	10–30	275–322			184–204		31.1–32.1
					type D quartz vein	i-1	10–30	274–371	–2.4 to –3.7			
i-2	60–80					301–335						
ii-2	10–30				269–300			213–249		32.6–34.7		
type b quartz vein	i-1			10–40	290–453	–2.8 to 12.3				4.7–16.2		
	i-2			70–80	295–341							
ii-1	10–40			269–459				204–356	32.1–43.0			
type c quartz vein	i-1			20–40	264–356	–1.2 to –4.2				2.1–6.7		
	i-2			60–80	258–359							
ii-1	20–40			271–385				246–272	34.5–36.1			
type II wollastonite vein	i-1			10–40	252–404	–5.8 to 17.4				9.0–20.5		
	i-2			60	341							
	ii-1			15	336				286	37.1		
	type III quartz vein			i-1	10–30	260–389						
				i-2	60–70	307–386	–0.9 to –2				1.6–3.4	
	ii-1			10–30	268–377				178–272	30.8–36.2		
type IV quartz vein	i-1			5–40	237–378	–6.8 to 17.4				10.2–20.5		
	i-2			70	286–360							
ii-1	20–40			237–350					191–252	31.5–34.9		
ii-2	20–40			297–336				189–215		31.4–32.7		
type I quartz vein	i-1			5–40	224–389	–1.2 to 21.2				2.1–23.2		
	i-2			50–70	240–386	–0.6 to –2				1.1–3.4		
	ii-1	10–40	237–377				173–272	30.6–36.9				
	ii-2	10–40	259–351				154–230	29.9–33.5				
Periphery	type I quartz vein	i-1	5–40	210–379	–1.5 to –20.1				2.6–22.5			
		i-2	50–70	225–386	–0.8 to –3.1				1.4–5.1			
		ii-1	20–40	332–371				221–234	33.0–33.7			
		ii-2	10–30	266–369				199–254	31.8–34.9			

Note: T_h -Homogenization Temperature; T_{ice} -Final ice melting temperature; T_s -Solid dissolution temperature for type ii-1 fluid inclusions; T_v - Vapor disappearance temperature for ii-2 fluid inclusions.

temperatures of melt inclusions were in the 734–1080°C range within quartz phenocrysts of 14 porphyry samples, which gives some indication of the temperature of the pre-hydrothermal stage. Nevertheless, no microthermometric data of coexisting fluid inclusions was reported. It is usually considered that porphyry systems initially exsolve a single phase of low to moderate salinity liquid (Fournier, 1999; Rusk et al., 2004, 2008; Sillitoe, 2010). This single

phase may evolve into a two-phase fluid system consisting of hypersaline liquid (brine) and low-density vapor in most typical porphyry deposits at shallow depths (<4 km) (Fournier, 1999). This occurs as the single-phase liquid decompresses, cools or intersects its solvus (Henley and McNabb, 1978; Burnham, 1979; Cline and Bodnar, 1991; Webster, 1992). Our results show that fluid inclusions in the Jiama deposit have recorded at least two boiling events

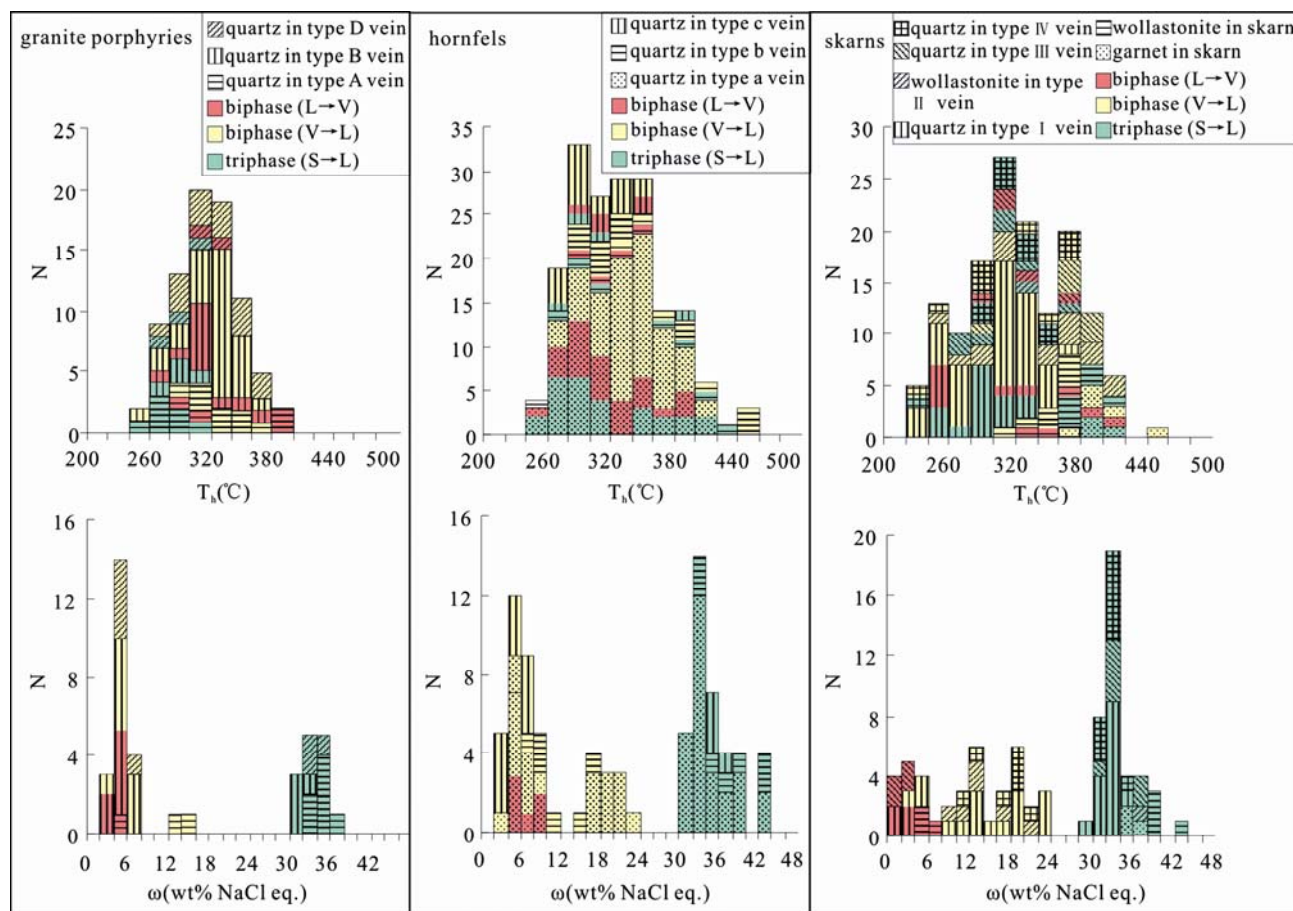


Fig. 7. Homogenization temperature and salinity histograms of fluid inclusions in minerals from porphyries, hornfels and skarns, Jiama deposit.

that took place in the hydrothermal stages.

In the early hydrothermal stage, the first boiling took place, inferred from the coexistence of liquid- and vapor-dominated fluid inclusions in wollastonite of the skarns, type A quartz veins in the porphyry and type a veins in the hornfels (Fig. 6a–b, g–h). Fluid evolution led to development of a vapor phase in the 245–417°C temperature range, a low to moderate salinity (0.9–22.5 wt%) liquid phase in the 243–455°C temperature range, and a high-salinity (30.2–43.4 wt%) liquid phase in the 240–418°C temperature range (Table 1, Fig. 8). The second boiling event took place in the late hydrothermal stage, inferred from the coexistence of liquid- and vapor-dominated fluid inclusions in type B quartz veins in the porphyries, type I veins in the skarns and type c veins in the hornfels (Fig. 6c–f, i–j). This boiling event is also inferred from the brecciated skarns and stockwork structures in the hornfels (Fig. 3i–j), which are consistent with sudden release of overpressured fluid. Fluid evolution in this late hydrothermal stage led to development of a vapor phase in the 225–386°C temperature range, a low to moderate salinity (2.1–23.2 wt%) liquid phase in the 210–453°C temperature range,

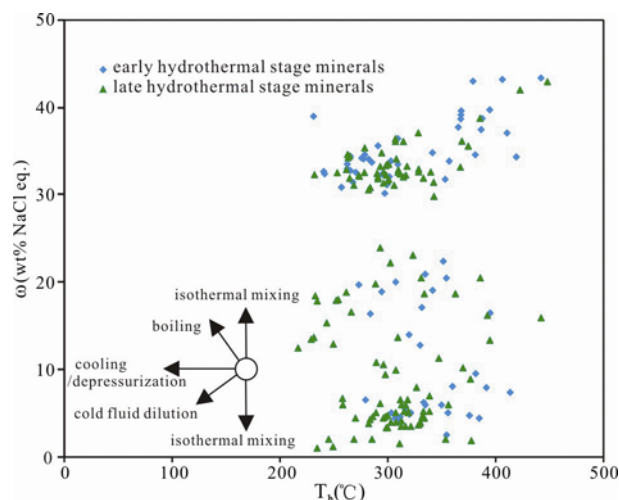


Fig. 8. Fluid inclusion homogenization temperature-salinity diagram of different stages, Jiama deposit.

and a high-salinity (29.9–43.0wt%) liquid phase in the 237–459°C temperature range (Table 1, Fig. 8). Guo Wenbo et al. (2014) made a H-O isotope study of quartz in three types of veins in hornfels and skarns, corresponding to type a, type b/c and type I veins in this paper. The δD and $\delta^{18}O_{H_2O}$ data show a trend of groundwater mixing with

magmatic fluid in the late hydrothermal stage (Fig. 11), suggesting that the second boiling event was accompanied by groundwater mixing.

Fluid inclusion microthermometry can be used to indicate fluid flow direction and potentially the sources of ore-forming fluids. For porphyry systems, the trend of decreasing fluid inclusion homogenization temperatures away from the magmatic intrusions is apparent (Chi Guoxiang, 2015). The two boiling events in the Jiama deposit appear to differ spatially in terms of fluid temperature and salinity. The first boiling event recorded by type a veins occurred mostly within lines 7–0–40, and shows a tendency of decreasing fluid inclusion abundance and salinity from the center to the periphery of the deposit (Fig. 9). The second boiling event, recorded by type I veins, occurred along the interlayered structural zones between hornfels and marble, with similar homogenization temperature and salinity characteristics from the center to the periphery (Fig. 10). The second boiling event does not show the common trend of porphyry systems as discussed above, and may be related to depressurization that caused

rapid outward fluid flow, similar to ore-forming fluids within the 4000 m vertical interval of the Sanshandao deposit (Jiang Xiaohui, et al., 2011; Wen et al., 2016).

5.2 Ore-forming mechanism

The resources presently identified in the Jiama deposit are distributed primarily in skarns (57%) and hornfels (40%) with only 3% hosted in porphyries. Core logs show that type B and D veins contribute to more than 2% of the mineralization in porphyries, type b and c veins contribute to more than 35% the mineralization in hornfels, type I veins contribute to more than 45% of the mineralization in skarns and type II, III and IV veins contribute to approximately 15% of the overall mineralization. As discussed above, the fluid inclusions in quartz from these veins indicate that fluid boiling took place in the second hydrothermal stage, and the H-O isotopes of quartz from different types of veins in hornfels and skarns suggest that magmatic fluid mixed with groundwater. The second fluid boiling, together with groundwater mixing, led to a temperature and salinity decrease, and an increase in pH,

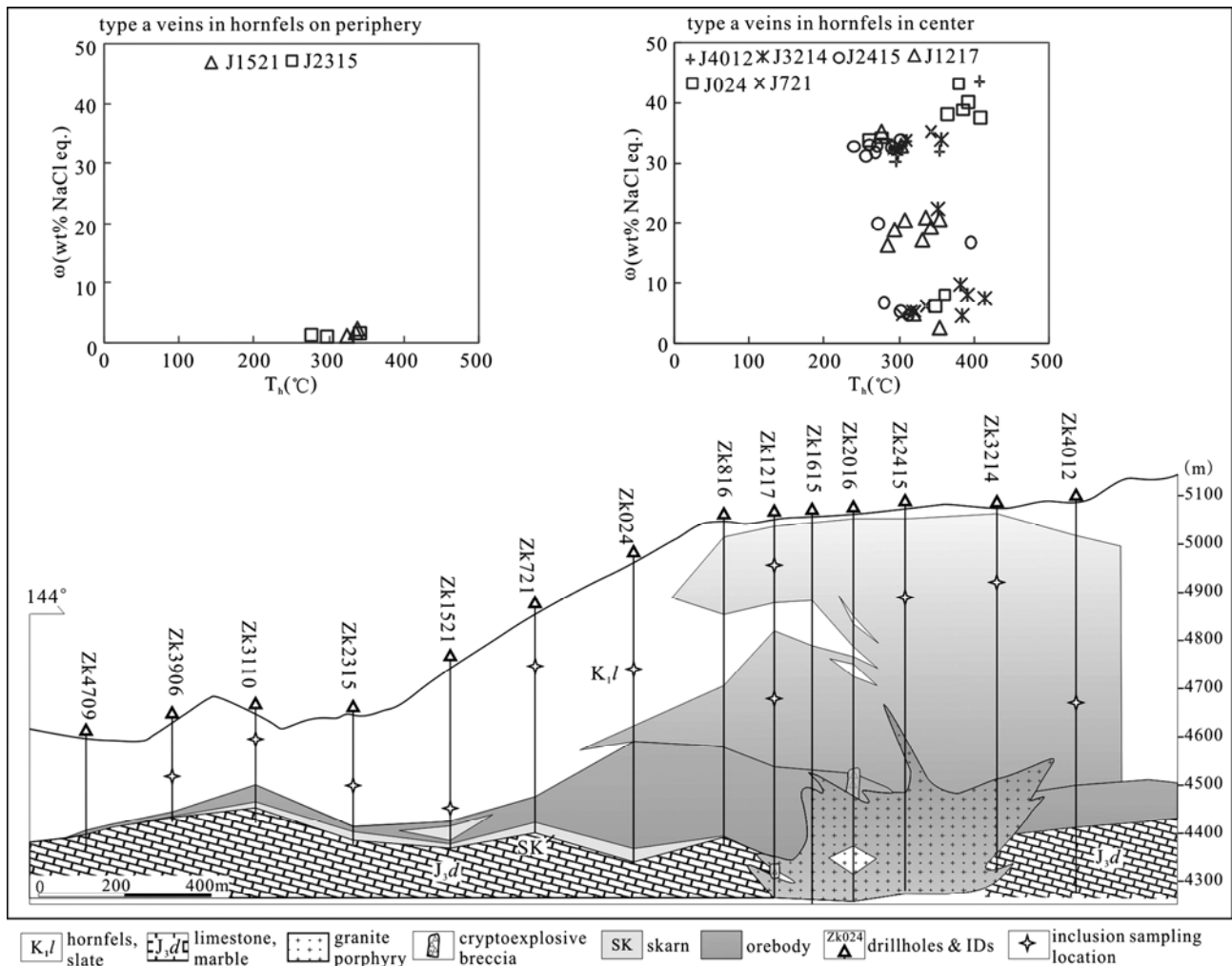


Fig. 9. Longitudinal section with temperature-salinity comparison between center and periphery for type a veins.

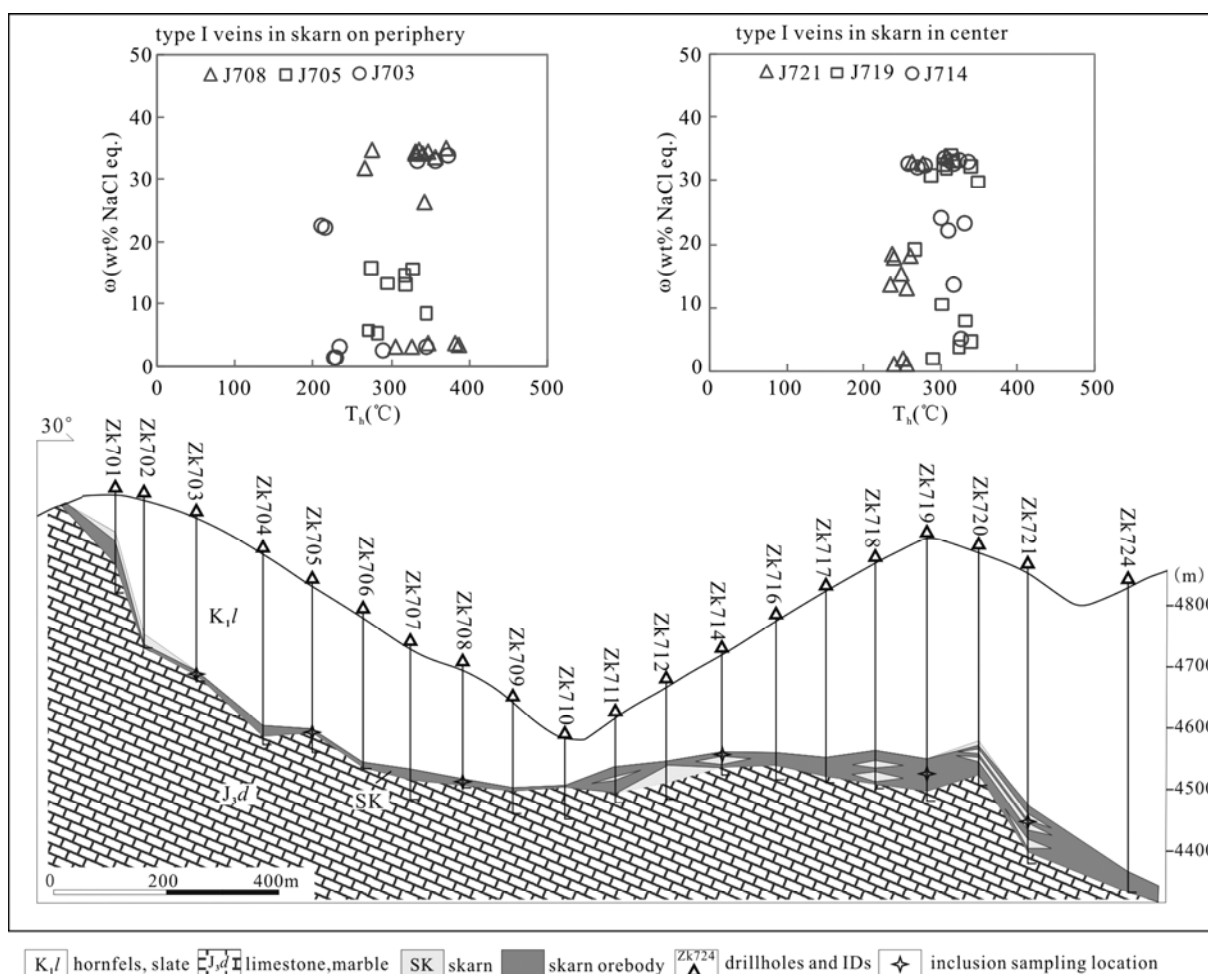


Fig. 10. Line 7 section with temperature-salinity comparison between the center and periphery for type I veins.

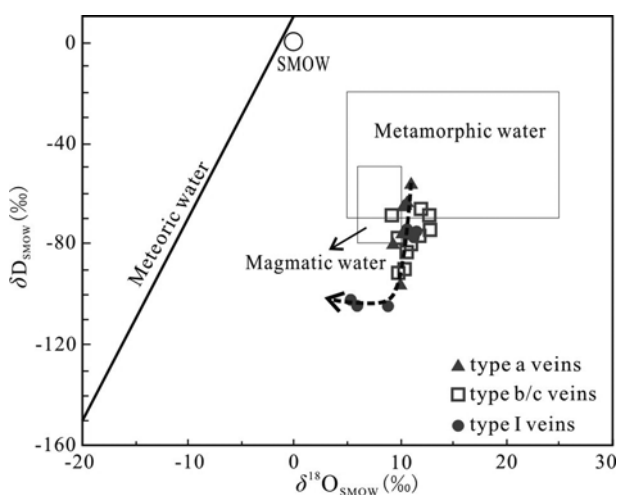


Fig. 11. δD - $\delta^{18}O$ diagram of quartz in different type of veins from Jiama deposit (base map is from Taylor, 1974; data are from Guo Wenbo et al., 2014).

all of which resulted in precipitation of ore minerals.
 Ore-forming elements display a zonation from the deposit center to its periphery: Mo→Mo (Cu)→Cu (Mo)→Cu (Pb + Zn + Mo)→ Cu (Pb + Zn) →Pb + Zn (Au)

(Tang Jvxing et al., 2010; Zheng Wenbao et al., 2011; Yao Xiaofeng et al., 2014a). Fluid inclusions from the late hydrothermal stage demonstrate that mineralization was mainly related to the second boiling event, as commonly recorded from the center to the periphery. This suggests that the mineral zonation was determined by the position to which elements migrated during boiling. The migration patterns of metallic elements are key factors in the formation of porphyry systems, and previous studies have confirmed that Au and Cu are preferentially partitioned into the vapor phase (Heinrich et al., 1999; Baker et al., 2004; Williams-Jones and Heinrich, 2005; Nagaseki and Hayashi, 2008; Lu Huanzhang and Shan Qiang, 2015). In the liquid phase, Fe, Zn, Pb and some Cu probably migrated in the form of Cl^- complexes (Heinrich et al., 1999; Nagaseki and Hayashi, 2008; Lu Huanzhang and Shan Qiang, 2015). Molybdenum probably migrated in the form of $MoO_2Cl_n^{2-n}$ complexes or MoO_4^{2-} anions (Ulrich and Mavrogenes, 2008). The second boiling event led to local decomposition of complexes that migrated to different positions, and variable complexes precipitated in different temperature ranges, resulting in zonation of the

ore-forming elements.

6 Conclusions

Based on the study presented regarding fluid inclusions and ore-forming processes in the Jiama deposit, the following conclusions can be drawn:

(1) Fluid evolution of the Jiama deposit involved at least two fluid boiling events. The first boiling event took place in the early hydrothermal stage, as recorded in type A veins in porphyries, type a veins in hornfels and wollastonite grains in skarns. The second boiling event occurred in the late hydrothermal stage, as recorded in type B and D veins in porphyries, type I, II, III and IV veins in skarns and type b and c veins in hornfels.

(2) The second fluid boiling event, and associated meteoric water mixing, is closely related to mineralization, contributing to more than 90% of the reserves in the deposit. The inclusions entrapped in type I veins from the center to the periphery within skarns indicate that the second boiling occurred along the interlayered structural zones between hornfels and marble. Moreover, variable element migration pathways and precipitation temperatures of Cu, Mo, Pb, Zn, Au and Ag resulted in ore-element zonation.

Acknowledgements

This work was funded by the third subject of National Natural Science Foundation of China (41302060), Geological Survey Project (12120114001304, 121201004000150012). We thank Tibet Huatailong Mining Development Co., Ltd. for support during the field studies. We thank Ding S. and Lin B. for their assistance in the field. We thank Warwick Hastie, PhD, from Liwen Bianji, Edanz Group China, for editing the English text of a draft of this manuscript. Thanks are also due to an anonymous reviewer and Prof. Chi Guoxiang of the University of Regina for critical and constructive comments which greatly improved the manuscript.

Manuscript received Dec. 2, 2016
accepted Apr. 19, 2017
edited by Fei Hongcai

References

- Baker, T., Van Achtenberg, E., Ryan, C.G., and Lang, J.R., 2004. Composition and evolution of ore fluids in a magmatic-hydrothermal skarn deposit. *Geology*, 32(2): 117–326.
- Burnham, C.W., 1979. *Magnas and hydrothermal fluids*, in Barnes, H.L., ed., *Geochemistry of hydrothermal ore deposits* (2nd ed.). New York: John Wiley & Sons, 71–136.
- Cannell, J., 2005. Mineralization, alteration, and structural evolution of the El Teniente porphyry Cu-Mo deposit. *Economic Geology*, 100(5): 979–1003.
- Chi Guoxiang and Lu Huanzhang, 2008. Validation and representation of fluid inclusion microthermometric data using the fluid inclusion assemblage (FIA) concept. *Acta Petrologica Sinica*, 24(9): 1945–1953 (in Chinese with English abstract).
- Chi Guoxiang, 2015. Constraints from fluid inclusion studies on hydrodynamic models of mineralization. *Acta Petrologica Sinica*, 31(4): 907–917.
- Cline, J.S., and Bodnar, R.J., 1991. Can economic porphyry copper mineralization be generated by a “typical” calc-alkaline melt? *Journal of Geophysical Research*, 96(B5): 8113–8126.
- Chung, S.L., Liu Dunyi, Ji Jiangqing, Chu Meifei, Lee, H.Y., Wen, D.J., Lo, C.H., Lee, T.Y., Qian Qing and Zhang Qi, 2003. Adakites from continental collision zones: melting of thickened lower crust beneath southern Tibet. *Geology*, 31(11): 1021–1024.
- Dilles, J.H., and Einaudi, M.T., 1992. Wall-rock alteration and hydrothermal flow paths about the Ann-Mason porphyry copper deposit, Nevada—a 6-km vertical reconstruction. *Economic Geology*, 87(8): 1963–2001.
- Duan Jilin, Tang Juxing, Mason, R., Zheng Wenbao and Ying Lijuan, 2014. Zircon U-Pb age and deformation characteristics of the Jiama porphyry copper deposit, Tibet: implications for relationships between mineralization, structure and alteration. *Resource Geology*, 64(64): 316–331.
- Fournier, R.O., 1999. Hydrothermal processes related to movement of fluid from plastic into brittle rock in the magmatic-epithermal environment. *Economic Geology*, 94(8): 1193–1211.
- Gao Yiming, Chen Yuchuan, Tang Jvxing, Li Chao, Li Xinfu, Gao Ming and Cai Zhichao, 2011. Re–Os dating of molybdenite from the Yaguila porphyry molybdenum deposit in Gongbo’gyamda area, Tibet, and its geological significance. *Geological Bulletin of China*, 30(7): 1027–1036 (in Chinese with English abstract).
- Gao Yongfeng, Hou Zengqian, Kamber, B.S., Wei Ruihua, Meng Xiangjin and Zhao Rongsheng, 2007. Adakite-like porphyries from the southern Tibetan continental collision zones: evidence for slab melt metasomatism. *Contributions to Mineralogy and Petrology*, 153(1): 105–120.
- Goldstein, R.H., and Reynolds, T.J., 1994. Systematics of fluid inclusions in diagenetic minerals. *SEPM Short Course*, 31: 199.
- Guo Wenbo, Zheng Wenbao, Tang Jvxing, Ying Lijuan, Wang Yiyun and Lin Bin, 2014. Geochemical constraints on the source of metallogenic fluids and materials in the Jiama polymetallic Cu deposit, Tibet. *Geology in China*, 41(2): 510–528 (in Chinese with English abstract).
- Gustafson, L.B., 1995. Patterns of mineralization and alteration below the porphyry copper orebody at El Salvador, Chile. *Economic Geology*, 90(1): 2–16.
- Hall, D.L., Sterner, S.M., and Bodnar, R.J., 1988. Freezing point depression of Na-KCl-H₂O solutions. *Economic Geology*, 83: 197–202.
- Harris, A.C., Kamenetsky, V.S., White, N.C., Achtenbergh, E.V., and Ryan, C.G., 2003. Melt inclusions in veins: linking magmas and porphyry Cu deposits. *Science*, 302(5653): 2109–2111.

- Harris, A.C., Kamenetsky, V.S., White, N.C., and Steele, D.A., 2004. Volatile phase separation in silicic magmas at Bajo de la Alumbrera porphyry Cu-Au deposit, NW Argentina. *Resource Geology*, 54(3): 341–356.
- Henley, R.W., and McNabb, A., 1978. Magmatic vapor plumes and groundwater interaction in porphyry copper emplacement. *Economic Geology*, 73: 1–20.
- Heinrich, C.A., Günther, D., Audétat, A., Ulrich, T., and Frischknecht, R., 1999. Metal fractionation between magmatic brine and vapor, determined by microanalysis of fluid inclusions. *Geology*, 27(8): 755–758.
- Hou Zengqian, Gao Yongfeng, Qu Xiaoming, Rui Zongyao and Mo Xuanxue, 2004. Origin of adakitic intrusives generated during mid-miocene east-west extension in southern Tibet. *Earth and Planetary Science Letters*, 220(1–2): 139–155.
- Hou Zengqian, Zhang Hongrui, Pan Xiaofei and Yang Zhiming, 2011. Porphyry Cu (–Mo–Au) deposits related to melting of thickened mafic lower crust: examples from the eastern Tethyan metallogenic domain. *Ore Geology Reviews*, 39(1–2): 21–45.
- Huang Wenting, Liang Huaying, Wu Jing, Wang Chunlong, Zou Yinqiao, Wang Xiuzhang, Xu Jifeng and Allen, C.M., 2013. Study on the metallogenesis during the early stage of continental collision in southern Gangdese, Tibet. *Acta Petrologica Sinica*, 29(4): 1439–1449 (in Chinese with English abstract).
- Huang Yong, Li Guangming, Ding Jun, Dai Jie, Yan Guoqiang, Dong Suiliang and Huang Hanxiao, 2017. Origin of the newly discovered Zhunuo porphyry Cu-Mo-Au deposit in the western part of the Gangdese porphyry copper belt in the southern Tibetan plateau, SW China. *Acta Geologica Sinica* (English Edition), 91(1): 109–134.
- Jiang Xiaohui, Fan Hongrui, Hu Fangfang, Yang Kuifeng, Lan Tingguang, Zheng Xiaoli and Jin Nianxian, 2011. Comparative studies on fluid inclusion in different depths and ore genesis of the Sanshandao gold deposit, Jiaodong Peninsula. *Acta Petrologica Sinica*, 27(5): 1327–1340 (in Chinese with English abstract).
- Lang Xinghai, Tang Juxing, Li Zhijun, Huang Yong, Ding Feng, Yang Huanhuan, Xie Fuwei, Zhang Li, Wang Qin and Zhou Yun, 2014. U-Pb and Re-Os geochronological evidence for the Jurassic porphyry metallogenic event of the Xiongcu district in the Gangdese porphyry copper belt, southern Tibet, PRC. *Journal of Asian Earth Sciences*, 79(2): 608–622.
- Leng Qiufeng, Tang Juxing, Zheng Wenbao, Lin Bin and Tang Pan, 2014. Geological features of the Jiama porphyry deposit in Tibet. *Acta Geologica Sinica* (English Edition), 88(supp. 2): 549–550.
- Li Guangming and Rui Zongyao, 2004. Diagenetic and mineralization ages for the porphyry copper deposits in the Gandise Metallogenic Belt, southern Tibet. *Geotectonica et Metallogenia*, 28(2): 165–170 (in Chinese with English abstract).
- Lu Huanzhang and Shan Qiang, 2015. Composition of ore forming fluids in metal deposits and fluid inclusion. *Acta Petrologica Sinica*, 31(4): 1108–1116 (in Chinese with English abstract).
- Mao Jinwen, Pirajno, F., Lehmann, B., Luo Maocheng and Berzina, A., 2014. Distribution of porphyry deposits in the Eurasian continent and their corresponding tectonic settings. *Journal of Asian Earth Sciences*, 79(2): 576–584.
- Meng Xiangjin, Hou Zengqian, Gao Yongfeng, Huang Wei, Qu Xiaoming and Qu Wenjun, 2003. Re-Os dating for molybdenite from Qulong porphyry copper deposit in Gangdese metallogenic belt, Tibet and its metallogenic significances. *Geological Review*, 49(6): 660–666 (in Chinese with English abstract).
- Nagaseki, H., and Hayashi, K., 2008. Experimental study of the behavior of copper and zinc in a boiling hydrothermal system. *Geology*, 36(1): 27–30.
- Pei Yingru, Sun Qingzhong, Zheng Yuanchuan, Yang Zhusen, Li Wei and Huang Kexian, 2016. Genesis of the Bangbu orogenic gold deposit, Tibet: evidence from fluid inclusion, stable isotopes, and Ar-Ar geochronology. *Acta Geologica Sinica* (English Edition), 90(2): 722–737.
- Qin Zhipeng, Wang Xiongwu, Dorji, Tang Juxing, Zhou Yun and Peng Huijuan, 2011. LA-ICP-MS U-Pb zircon age of intermediate-acidic intrusive rocks in Jiama of Tibet and its metallogenic significance. *Mineral Deposit*, 30(2): 339–348 (in Chinese with English abstract).
- Qu Xiaoming, Hou Zengqian, Zaw, K., and Li Youguo, 2007. Characteristics and genesis of Gangdese porphyry copper deposits in the southern Tibetan Plateau: preliminary geochemical and geochronological results. *Ore Geology Reviews*, 31(1–4): 205–223.
- Rui Zongyao, Hou Zengqian, Qu Xiaoming, Zhang Lisheng, Wang Longsheng and Liu Yulin, 2003. Metallogenic epoch of Gangdese porphyry copper belt and uplift of Qinghai-Tibet Plateau. *Mineral Deposits*, 22(3): 217–225 (in Chinese with English abstract).
- Rusk, B.G., Reed, M.H., Dilles, J.H., Klemm, L.M., and Heinrich, C.A., 2004. Compositions of magmatic hydrothermal fluids determined by LA-ICP-MS of fluid inclusions from the porphyry copper-molybdenum deposit at Butte, MT. *Chemical Geology*, 210(1–4): 173–199.
- Rusk, B.G., Reed, M.H., and Dilles, J.H., 2008. Fluid inclusion evidence for magmatic-hydrothermal fluid evolution in the porphyry copper-molybdenum deposit at Butte, Montana. *Economic Geology*, 103(2): 307–334.
- Sillitoe, R.H., 2010. Porphyry copper systems. *Economic Geology*, 105(1): 3–41.
- Sun Xiang, Zheng Youye, Wu Song, You Zhimin, Wu Xu, Li Miao, Zhou Tiancheng and Dong Jun, 2013. Mineralization age and petrogenesis of associated intrusions in the Mingze-Chengba porphyry-skarn Mo-Cu deposit, Gangdese. *Acta Petrologica Sinica*, 29(4): 1392–1406 (in Chinese with English abstract).
- Tang Juxing, Dorji, Liu Hongfei, Lang Xinghai, Zhang Jinshu, Zheng Wenbao and Yi Lijuan, 2012. Minerogenetic series of ore deposits in the east part of the Gangdise Metallogenic Belt. *Acta Geoscientica Sinica*, 33(4): 393–410 (in Chinese with English abstract).
- Tang Jvxing, Lang Xinghai, Xie Fuwei, Gao Yiming, Li Zhijun, Huang Yong, Ding Feng, Yang Huanhuan, Zhang Li, Wang Qin and Zhou Yun, 2015. Geological characteristics and genesis of the Jurassic No. I porphyry Cu–Au deposit in the Xiongcu district, Gangdese porphyry copper belt, Tibet. *Ore Geology Reviews*, 70(4): 94–95.
- Tang Jvxing, Wang Denghong, Wang Xiongwu, Zhong Kanghui, Ying Lijuan, Zheng Wenbao, Li Fengji, Guo Na, Qin Zhipeng, Yao Xiaofeng, Li Lei, Wang You and Tang Xiaoqian, 2010. Geological features and metallogenic model of the Jiama

- copper-polymetallic deposit in Tibet. *Acta Geoscientia Sinica*, 31(4): 495–506 (in Chinese with English abstract).
- Tang Jvxing, Zheng Wenbao, Chen Yuchuan, Wang Denghong, Ying Lijuan and Qin Zhipeng, 2013. Prospecting breakthrough of the deep porphyry ore body and its significance in Jiama copper polymetallic deposit, Tibet, China. *Journal of Jilin University (Earth Science Edition)*, 43 (4): 1100–1110 (in Chinese with English abstract).
- Taylor, H.P.J., 1997. Oxygen and hydrogen isotope relationships in hydrothermal mineral deposits. *Geochemistry of Hydrothermal Ore Deposits*, 2: 236–277.
- Ulrich, T., and Mavrogenes, J., 2008. An experimental study of the solubility of molybdenum in H₂O and KCl-H₂O solutions from 500°C to 800°C, and 150 to 300 MPa. *Geochimica Et Cosmochimica Acta*, 72(9): 2316–2330.
- Wang Baodi, Guo Lin, Wang Liquan, Li Bing, Huang Hanxiao, Duan Zhiming and Zeng Qinggao, 2012. Geochronology and petrogenesis of the ore-bearing pluton in Chagele deposit in middle of the Gangdese Metallogenic Belt. *Acta Petrologica Sinica*, 28(5): 1647–1662 (in Chinese with English abstract).
- Wang Denghong, Tang Juxing, Ying Lijuan, Lin Bin and Ding Shuai, 2011. Hornfels feature in the Jiama ore deposit, Tibet and its significance on deep prospecting. *Acta Petrologica Sinica*, 27(7): 2103–2108 (in Chinese with English abstract).
- Wang Liqiang, Cheng Wenbin, Tang Juxing, Kang Haoran, Zhang Yan and Zhuang Li, 2015. U–Pb geochronology, geochemistry, and H–O–S–Pb isotopic compositions of the Leqingla and Xin'gaguo skarn Pb–Zn polymetallic deposits, Tibet, China. *Journal of Asian Earth Sciences*, 115: 80–96.
- Webster, J.D., 1992. Fluid-melt interactions involving Cl-rich granites: Experimental study from 2 to 8 kbar. *Geochimica et Cosmochimica Acta*, 56: 659–678.
- Wen Bojie, Fan Hongrui, Hu Fangfang, Liu Xuan, Yang Kuifeng and Sun Zongfeng, 2016. Fluid evolution and ore genesis of the giant Sanshandao gold deposit, Jiaodong gold province, China: constraints from geology, fluid inclusions and H–O–S–He–Ar isotopic compositions. *Journal of Geochemical Exploration*, 171: 96–112.
- Williams-Jones, A.E., and Heinrich, C.A., 2005. Vapor transport of metals and the formation of magmatic- hydrothermal ore deposits. *Economic Geology*, 100(7): 1287–1312.
- Xu Jing, Zheng Youye, Sun Xiang and Shen Yahui, 2016. Geochronology and petrogenesis of miocene granitic intrusions related to the Zhibula Cu skarn deposit in the Gangdese Belt, southern Tibet. *Journal of Asian Earth Sciences*, 120: 100–116.
- Yao Xiaofeng, Ye Tianzhu, Tang Jvxing, Zheng Wenbao, Ding Shuai, Li Yongsheng and Zhen Shiming, 2014a. The effect of Si–Ca interface on skarn formation and polymetallic mineralization in the Jiama deposit, Tibet. *Geology in China*, 41(05): 1577–1593 (in Chinese with English abstract).
- Yao Xiaofeng, Tang Juxing, Ding Shuai, Zheng Wenbao, Zhang Wanyi and Shan Liang, 2014b. Genesis and main differences of Jiama and Qulong super-large deposit in Gangdese Metallogenic Belt. *Acta Geologica Sinica (English Edition)*, 88(supp. 2): 633–634.
- Ying Lijuan, Tang Juxing, Wang Denghong, Chang Zhesheng and Zheng Wenbao, 2009. Re–Os isotopic dating of molybdenite in skarn from the Jiama copper polymetallic deposit of Tibet and its metallogenic significance. *Rock and Mineral Analysis*, 28(3): 265–268 (in Chinese with English abstract).
- Ying Lijuan, Tang Juxing, Wang Denghong, Zheng Wenbao, Qin Zhipeng and Zhang Li, 2011. Zircon shrimp U–Pb dating of porphyry vein from the Jiama copper polymetallic deposit in Tibet and its significance. *Acta Petrologica Sinica*, 27(7): 2095–2102 (in Chinese with English abstract).
- Ying Lijuan, Wang Chenghui, Tang Juxing, Wang Denghong, Qu Wenjun and Li Chao, 2014. Re–Os systematics of sulfides (chalcopyrite, bornite, pyrite and pyrrotite) from the Jiama Cu–Mo deposit of Tibet, China. *Journal of Asian Earth Sciences*, 79(2): 497–506.
- Yu Yushuai, Yang Zhusen, Liu Yingchao, Tian Shihong, Ji Xianhua, Gao Yuan, Zhao Can, Zhao Wuqiang and Liu Aisui, 2012. Mineralogical characteristics and ⁴⁰Ar–³⁹Ar dating of phlogopite from the Gunjiu iron deposit in the Nixiong Ore Field, Coqen, Tibet. *Acta Petrologica Et Mineralogica*. 31(5): 681–690 (in Chinese with English abstract).
- Zeng Zhongcheng, Liu Demin, Wang Mingzhi, Zeren Zaxi, Ciren Nima, Zhang Ruoyu, Chen Ning and Zhu Weipeng, 2016. Tectonic-magmatic evolution and mineralization of the Qulong–Jiama areas in eastern section of Gangdese Mountains, Xizang (Tibet). *Geological Review*, 62(3): 663–678 (in Chinese with English abstract).
- Zhao Junxing, Qin Kezhang, Li Guangming, Cao Mingjian, Evans, N.J., McInnes, B.I.A., Li Jinxiang, Xiao Bo and Chen Lei, 2015a. The exhumation history of collision-related mineralizing systems in Tibet: insights from thermal studies of the Sharang and Yaguila deposits, central Lhasa. *Ore Geology Reviews*, 65(1): 1043–1061.
- Zhao Junxing, Qin Kezhang, Xiao Bo, McInnes, B., Li Guangming, Evans, N., Cao Mingjian and Li Jinxiang, 2015b. Thermal history of the giant Qulong Cu–Mo deposit, Gangdese metallogenic belt, Tibet: Constraints on magmatic-hydrothermal evolution and exhumation. *Gondwana Research*, 34(1): 1207–1211.
- Zhao Xiaoyan, Yang Zhusen, Zheng Yuanchuan, Liu Yingchao, Tian Shihong and Fu Qiang, 2015. Geology and genesis of the post-collisional porphyry–skarn deposit at Bangpu, Tibet. *Ore Geology Reviews*, 70: 486–509.
- Zheng Wenbao, Chen Yuchuan, Song Xin, Tang Juxing, Ying Lijuan, Li Fengji and Tang Xiaoqian, 2010. Element distribution of Jiama copper-polymetallic deposit in Tibet and its significance. *Mineral Deposits*, 29(5): 775–784 (in Chinese with English abstract).
- Zheng Youye, Sun Xiang, Gao Shunbao, Wu Song, Xu Jing, Jiang Junsheng, Chen Xin, Zhao Zhongying and Liu Yan, 2015. Metallogenesis and the minerogenetic series in the Gangdese polymetallic copper belt. *Journal of Asian Earth Sciences*, 103: 23–39.
- Zhong Kanghui, Li Lei, Zhou Huiwen, Bai Jingguo, Li Wei, Zhong Wanting, Zhang Yongqiang, Lin Jiqing, Zheng Fanshi, Huang Xiaoyu, Lu Biao and Lei Bo, 2012. Features of Jiama (Gyama)-Kajunguo thrust-gliding nappe tectonic system in Tibet. *Acta Geoscientia Sinica*, 33(4): 411–423 (in Chinese with English abstract).
- Zhou Yun, Wang Xiongwu, Tang Jvxing, Qin Zhipeng, Peng Huijuan, Li Aiguo, Yang Ke, Wang Hua, Li Jiong and Zhang Jichao, 2011a. Composition of single melt inclusion in quartz phenocryst in the Jiama Cu-polymetallic deposit. *Journal of Chengdu University of Technology (Natural Science Edition)*, 38(1): 92–102 (in Chinese with English abstract).

Zhou Yun, Wang Xiongwu, Tang Juxing, Qin Zhipeng, Peng Huijuan, Li Aiguo, Yang Ke, Wang Hua, Li Jiong and Zhang Jichao, 2011b. Origin and evolution of ore-forming fluids from Jiama copper polymetallic deposit in Tibet. *Mineral Deposits*, 30(2): 231–248 (in Chinese with English abstract).

China University of Geosciences (Beijing); post-doctor in China University of Geosciences (Beijing), senior geologist in the Development and Research Center, China Geological Survey (CGS), majoring in ore genesis and metallogeny. E-mail: 289332792@qq.com.

About the first author:

YAO Xiaofeng, male, born in 1986, doctor, graduated from